FINAL TECHNICAL REPORT

Submitted to

National Aeronautics and Space Administration

NASA Grant NGR 44-004-133

Our Account E1330

Prepared by:

F. R. Allum

March 1974

FINAL REPORT

NGR 44-004-133

1.0 INTRODUCTION

As outlined below, a number of investigations of cosmic ray

anisotropies and their relationship to concurrent magnetic field data have

been made during the tenure of this grant. These investigations have ranged

in scope from the examination of data very late in the decay phase of a solar

particle event where long term ($\sim$ 6 hour) averages are used and definite

interplanetary effects sought after to an examination of the change in low

energy particle anisotropy as the satellite approaches the bow shock and

the magnetopause.

1.1 General Data Information

The particle data presented in these analyses were obtained from the

University of Texas at Dallas (UTD) cosmic ray experiments on Explorers 34

and 41. A description of the instruments together with the general data

handling procedures and energy channels available is given elsewhere (Allum

et al 1971, Bartley et al 1971, Rao et al, 1971). Briefly, the instrument

is mounted perpendicular to the spin axis of the satellite and the counting

rate is obtained from eight, 45° sectors as the detector scans the plane of

the ecliptic. These normalised data samples are fitted to a sinusoid of the

form

$$A = A_o + A_1 \cos (\phi - \phi_{cr})$$

The anisotropy amplitude δ, after correcting for averaging effects, and

the azimuthal direction of maximum intensity of the first harmonic are given

by 1.026 (A_1/A_0) and ϕ_{cr} respectively.

2.0 THE LATE DECAY PHASE ANISOTROPY

Late in the decay phase of a solar flare event, the particle anisotropy is directed from the east at an azimuthal angle approximately 40° east of the sun-earth line. While this easterly anisotropy may develop some 3 or 4 days after the onset of the event, in order (a) to determine whether an easterly anisotropy has developed and (b) to study the phenomena of it as observed, one must obtain meaningful statistics over a long period- say, of order 8 days in the 0.7 - 7.6 MeV energy range. Consequently the study of this easterly anisotropy phase is restricted generally to the larger solar flare events and in particular to those events which are not contaminated by another particle injection during the decay phase. In paragraph 2.1, a summary is given of the conclusions reached from our study of 5 events in which an easterly anisotropy phase was observed in the data from the UTD experiments on Explorers 34 and 41. From the totality of data available to us during the course of this investigation, it is believed that the characteristics of this eastern anisotropy phase described in paragraph 2.1 are typical of all such eastern anisotropies and that the development of an eastern anisotropy phase is the normal pattern of behaviour provided the decay intensity can be followed for sufficient time. There are exceptions to this general rule so that the word 'normal' should not be interpreted too literally. In paragraph 2.2 one such exception is discussed in some detail.

2.1 Characteristics and Theoretical Implications of the

Eastern Anisotropy Phase

The anisotropy vector and decay time constant for cosmic-ray protons in the kinetic energy interval $0.7 \leq T \leq 7.6$ MeV have been examined late in a solar-flare event and have been compared with concurrent interplanetary magnetic field data. The principal results are summarized below:

(1) The anistoropy late in the solar-flare event is directed from the direction $38.7^{\circ} \pm 2.4^{\circ}$E ($\phi_{cr}^{*} = 321.3^{\circ}$) and this direction is independent of the concurrent local magnetic-field azimuth. The azimuth of the cosmic-ray anisotropy is not generally perpendicular to the local magnetic-field vector.

(2) This invariant direction is normal to the mean magnetic field direction within the statistical error of the available data ($\sim 5^{\circ}$).

(3) The amplitude of the easterly-directed cosmic-ray anisotropy is strongly dependent on the local magnetic-field vector increasing from 0.5% to $\sim$ 30% as the magnetic azimuth changes from 360° to 250°.

(4) The decay time constant is approximately inversely proportional to the anisotropy amplitude, and thus on the azimuth of the concurrent magnetic field vector.

(5) From consideration of the present data and our previously published data, it is concluded that the azimuth of the easterly anisotropy phase is invariant at $38.7 \pm 2.4^{\circ}$ East over a wide range of particle speed, $0.06 \leq \bar{\beta} \leq 0.56$, in contradiction to predictions of currently accepted models of solar-particle propagation.

(6) The analysis of the data confirms that, in each of the three identifiable phases of a solar flare event at these energies (i.e., early, radial, and easterly phases), the anisotropy is comprised of a radial convective component $\underline{\delta}_c$ and a diffusive component aligned with the magnetic field.

(7) The assumption that the late-time anisotropy is perpendicular to the nominal direction of Archimedes spiral everywhere in the solar cavity leads to an inconsistency with the currently accepted values of the interplanetary diffusion coefficient, viz, it requires a time decay constant of 50 hours compared with the observed value of around 20 hours.

(8) Deviations from the nominal Archimedes spiral structure have been treated as 'kinks' in the magnetic flux tubes which are convected out with the solar wind.

(9) The observations and (7) above lead us to suggest that at late times in an event, at any point $\underline{r}$ in the solar cavity, the bulk flow velocity of the cosmic-ray particles in the kink is such that its component in the direction of the mean magnetic field $\underline{e}_0$ remains constant independent of the concurrent magnetic-field direction $\underline{e}$, i.e.,

$$\underline{\delta} \cdot \underline{e}_0 = k(\underline{r})$$

the constant $k(\underline{r})$ being a function of position $\underline{r}$, with value zero near Earth.

(10) Based on (9) we deduce that $\kappa_{\parallel}'$, the parallel diffusion coefficient in the 'kinked' structure, is related to $\kappa_{\parallel}$ the nominal parallel diffusion coefficient, by

$$\kappa_{\parallel}' = \kappa_{\parallel} / \cos^2 (\psi - \psi_0)$$

with $\psi-\psi_0$ the angle between $\underline{e}$ and $\underline{e}_0$. This result appears to be the major

theoretical deduction we make from the observations reported herein.

(11) A theory relating the decay-time-constant variation to the

magnetic-field-azimuth variation from $\underline{e}_0$ has been derived. With this we

deduce a radial gradient of 1000%AU for the $0.7 \leq T \leq 7.6$ MeV interval and

a corresponding $\kappa_{\prime\prime}$ of 1.3×10^{20} $cm^2 sec^{-1}$.

2.2   The May 1972 Event

As indicated above, the characteristics of the late time anisotropy

described in paragraph 2.1 are believed to be of general validity, i.e.

if the decay of the event is not disturbed by a fresh injection of particles

then an eastern anisotropy will develop if the event can be followed for

sufficient duration. Furthermore, this eastern anisotropy is directed at

a constant azimuth of 38.7^o East of the sun-earth line for a wide range of

particle velocity and magnetic field azimuth. In this section, we discuss what

appears to be an interesting exception to this general behaviour pattern.

As may be seen from Figure 1, a significant particle injection

occurred in late May 1972 with a relatively smooth decay until 08 June

when a fresh injection of particles is detected. The variation in the

decay time around 04 May is probably associated with a sector boundary. The

period of interest for the present discussion begins around 0300 UT, 06

June and continues until 0300 UT, 08 June, i.e. some 10-12 days after the

onset of the event and thus at a time when a positive density gradient is

expected to be established. In Figures 2a, b we show the general relation

between the directions of the cosmic ray anisotropy and interplanetary

magnetic field for this period. Between 0300 UT; 06 June, 1972 and 0600

UT; 07 June, 1972 the particle anisotropy is directed from the west ($\sim 60^{\circ}$West)

while the magnetic field is in the eastern quadrants ($\phi_m \sim 40^{\circ}$E). Around

0700 UT; 07 June, 1972, the magnetic field changes to the general Archimedes

Spiral angle ($\sim 45^{\circ}$West). At the same time, the cosmic ray anisotropy

changes to a direction $\sim 50^{\circ}$ East. We have attempted to explain these

observations by assuming a positive density gradient resulting in an

inward diffusion of particles along the prevailing direction of the

interplanetary field line. The corresponding vector triangles showing the

convective and diffusive components together with the resultant particle

anisotropy are illustrated in Figures 2c, d.

A possible configuration of the interplanetary magnetic field is

shown in Figure 3. An observer located at X will see the magnetic field

structure convected outwards by the solar wind. Consequently during the

interval A B, the magnetic field will be directed in the eastern quadrants

while in the interval B C, the magnetic field will be generally in the

Archimedes Spiral direction.

As there is no sharp change in the intensity or the decay time of the

particle population at this time, the field configuration shown in Figure 3

and the vector triangles shown in Figures 2c, d, are consistent with the

particle data.

It should be emphasized that this is one example where due to a

particular type of field configuration, it could be possible to obtain a

western anisotropy (rather than an eastern) late in the decay phase of a

flare event. Such an observation is only possible if the magnetic

field is in the eastern quadrant as shown in Figure 3 (along A B). It

is unwise at this point with only one example to draw any general

conclusions. It is intended to search the totality of our experimental

data for additional examples to support this analysis. There is some

evidence for a similar effect on 07 November 1968 and 17 June 1968. However

these latter events will have to be considered in more detail before it can

be determined if they support the above analysis.

3.0 The June 1972 Events

In Figure 1, the relative counting rate in the broad proton energy

range 0.7 - 55 MeV is shown for the period 27 May - 24 June, 1972, while

the relative counting rate from the 7.6 - 55 MeV proton channel for the

period 08 June - 20 June, 1972 is shown in Figure 4.

In early June, 1972, there were two distinct injections of 7.6 - 55 MeV

protons as may be seen from Figure 4. For the 08 June event, it is not

possible to give a precise onset time for the particle increase as Explorer

41 was near perigee at this time and the detectors were recording magneto-

spheric particle fluxes at the beginning of the event. In setting possible

limits, the onset of the event definitely occurred after 0800 UT and prior

to 1700, 08 June. Following a rapid rise, this event displays several

marked variations in count rate around the time of maximum particle

intensity.

Figures 1 and 4 indicate that a small but statistically significant

increase in particle flux occurred at approximately 1430 UT, 14 June 1972.

However, the major increase in the 7.6 - 55 MeV proton flux did not occur

until around 0400 UT, 16 June, 1972. For the 0.7 - 7.6 MeV energy range,

after a small plateau region in the intensity profile, there is a steady increase in the particle flux prior to 0400 UT 16 June when a more rapid rise to maximum intensity commences. As discussed below 3.1, the anisotropic characteristics of the particle population prior and subsequent to 0400 UT 16 June differ significantly.

The dominant feature of the second particle increase in the 0.7 - 7.6 MeV channel is the energetic storm particle (ESP) event which occurred following the passage of the shock front across the spacecraft to produce the sudden commencement observed at the earth at 1312 UT, 17 June. This ESP event is discussed below (3.2).

3.1   Anisotropic Characteristics of the Particle Population

The temporal variations of the anisotropy amplitude and azimuth of the 0.7 - 7.6 MeV protons during the periods under investigation are shown in Figures 5 and 7. In these diagrams, we show the consecutive hourly averages (plotted vectorially) of the anisotropy vector $\bar{\delta}$, projected into the ecliptic plane.

The onset of the 08 June event is marked by a strong field aligned anisotropy (of order 90% from 80° W of the Earth-Sun line) of some 12 hours duration. The angular distribution in the plane of the ecliptic during one 10.9 minute interval (2019 - 2030 UT, 08 June) is shown in Figure 6(a). A well defined anisotropy, of amplitude $\sim 35\%$ directed $\sim 60^{\circ}$ West of the Earth-Sun line is observed to commence at 0400 UT, 10 June and lasts with slightly diminishing amplitude until at least 1600 UT, 11 June and probably until 1200 UT, 12 June. Visually, these measurements have the characteristics

of a field aligned anisotropy phase. However as may be seen from Figure 1, this time interval occurs during the decay phase of the 08 June event. During most of this time interval the satellite is located some distance away from the bow shock. At 0900 UT, 10 June, the spacecraft is located $X_{SE} = 25.3$ R_e; $Y_{SE} = 11.5$ R_e; $Z_{SE} = 4.4$ R_e while at 2200 UT, 10 June the coordinates are $X_{SE} = 21.6$ R_e; $Y_{SE} = 9.4$ R_e; $Z_{SE} = 6.9$ R_e. Both of these locations are outside of the average position of the bow shock for the 1963-1968 epoch (Fairfield 1971). It is highly improbable that this pronounced field-aligned anisotropy in the decay phase could be due to any interference arising from the proximity of the bow shock. In general, it is possible to follow a field aligned anisotropy inside the bow shock (see 5.1 below). When interference in the anisotropy measurements does occur due to the presence of the earth's magnetic field, it has been our experience that the anisotropy is destroyed (i.e. the particle flux becomes isotropic) rather than the reverse. Thus it is considered that the anisotropy shown in Figure 5 represents the true anisotropic character of the particle population in interplanetary space. A preliminary examination of the magnetic field data indicates that a sector boundary occurred around 2200 UT, 09 June. The observations made during this event are thus consistent with the conclusions drawn from our earlier study of the Explorer 34 data from the 1967 epoch viz, when the spacecraft is in the proximity of a sector boundary during the field-aligned phase of a solar proton event, this field aligned anisotropy can occur for an extended period of time, almost up to the end of the proton event.

Before 0400 UT, 16 June, i.e. in the plateau region for the 7.6 - 55 MeV protons and during the gradually rising portion of the 0.7 - 7.6 MeV proton profile, the amplitude of the particle anisotropy is small (of order 10%) and generally is directed from the east. Around 0400 UT, when the intensity of the 7.6 - 55 MeV protons begins to increase sharply, the amplitude of the particle anisotropy in the 0.7 - 7.6 MeV energy channel increases to a value of the order of 50%, directed from the west, to commence the field aligned phase of the event. The amplitude of the anisotropy measured during the field aligned phase of this 16 June particle event is not as pronounced as that observed in the 08 June event (c.f. Figures 5 and 7). A sample of the angular distribution in the plane of the ecliptic during one 10.9 minute interval (0841 - 0852 UT, 16 June) is shown in Figure 6(b). At the time of the sudden commencement (1321 UT, 17 June), there is a sudden shift in the anisotropy phase from a generally western direction to one from the east. This part of the event is discussed below(3.2) in the observations relating to the ESP event. Late in the decay phase (22 June - 26 June) an easterly anisotropy develops (McCracken et al, 1971, Rao et al, 1971, Allum et al, 1973, 1974). At this time, the counting rate from the detectors is relatively low and consequently there are significant statistical fluctuations in the data. However the general tendency for the particle anisotropy to be directed from the east is readily observed.

3.2   Energetic Storm Particle Event

A significant Forbush decrease was observed in the neutron monitor network on 17 June following the sudden commencement at 1312 UT on the same day. (Solar-Geophysical Data, page 117, #336, Part 1, 1972). The Forbush

decrease was observed also in the higher energy channels of the cosmic ray experiments on Explorer 41 (Solar-Geophysical Data, page 75, #340, Part 2, 1972). In the lower energy ranges there is an order of magnitude increase in the particle flux following the onset of the Forbush decrease. In Figure 8, intensity-time profiles for 3 different energy ranges viz 0.7 - 7.6 MeV, 7.6 - 55 MeV, and > 35 MeV, are shown for 14 hours around this time interval, and clearly illustrate the significant increase in particle flux detected in the low energy channels and the Forbush decrease in the >35 MeV data. In the low energy channel, the particle increase is of approximately 12-14 hours duration. Observations of similar particle increases have been reported in the literature (e.g. Bryant et al, 1962, 1965; Rao et al, 1967) and are generally referred to as energetic storm particle events.

Fine-time-scale anisotropy data (9.28 second samples taken at 81.92 second intervals) for the 0.7 - 7.6 MeV energy range are shown in Figure 9 for the time interval immediately preceeding and subsequent to the passage of the shock front across the satellite position. While the anisotropy amplitude remains esentially at the same average value throughout this period (excluding the 5 minute interval immediately preceeding the arrival of the shock front when a statistically significant increase in anisotropy amplitude and particle intensity are observed) clearly, there is a change in the direction of this anisotropy at the time the shock front passes the satellite location. The angular distributions in the plane of the ecliptic for two 10.9 minute intervals before and after the passage of the shock front are shown in Figures 6(c) and 6(d) respectively.

Anisotropy data from the 0.7 - 7.6 MeV energy range are not available throughout the duration of the energetic storm particle event due to saturation of this particular channel of the experiment around the time of maximum particle intensity. However during the rising portion of the event, the anisotropy is consistently directed from the east. A bi-directional anisotropy commences at 2008 UT, 17 June in both the 0.7 - 7.6 and 7.6 - 55 MeV energy channels. Angular distributions in the plane of the ecliptic for two 10.9 minute intervals during this time interval are shown in Figures 6 (e) and 6 (f) respectively. In general, the two maxima of the angular distributions during this period occur in octants 4 and 8, i.e. close to the sun and anti-sun direction respectively. The presence of bidirectional anisotropies following energetic storm particle events have been noted previously by Rao et al (1967) using data from Pioneers 6 and 7.

4.0   The Scatter Free Event of 20 April, 1971

While there are three distinct phases observed in the low energy particle anisotropy measurements following a large solar flare event, most of the analysis contained in recent papers has focused on the radial and easterly phases which occur late in the decay phase of the event. (e.g. Allum et al 1974). Only a relatively small amount of detailed analysis has been made on the initial field aligned anisotropy phase, and in particular on the decay rate of this initial anisotropy amplitude.

Diffusion theory (neglecting convection and energy loss) predicts that the anisotropy amplitude will decay as $1/vt$ (v is the particle velocity, t

is the time) after an impulsive injection of particles into a medium where the diffusion coefficient is described by $\kappa(r) = \kappa_0 r^\beta (\beta < 2)$ and where r is distance from the sun. The amplitude of the anisotropy is determined by β but is independent of κ_0. For example when $\beta = 0$ the anisotropy $\delta = 3r/2vt$. (Axford 1971, and references therein). Allum et al (1971) examined the decay of the field aligned anisotropy amplitude for the event of 03 June 1967 using low energy proton and electron data obtained from the UTD experiment on Explorer 34 and found that the experimental results were in good accord with the predictions of a $^1/vt$ dependence proposed by Fisk and Axford (1969). However, the anisotropy amplitudes of some low energy proton events decay at a much slower rate than the above theoretical predictions and in fact, some events exhibit large anisotropy amplitudes well beyond the normal expected time scale. The event described in this section (viz 20 April 1971) is one example of a large anisotropy amplitude being sustained well into the decay phase of the particle intensity.

Different proposals have been offered to explain these sustained anisotropy amplitudes which decay at a slower rate than that expected from simple diffusion models with $\beta = 0$. Using a Monte Carlo technique, Vernov et al (1969) investigated the temporal variation of the particle anisotropy and intensity at 1 AU following release of the particles from the sun over an extended period of time into the interplanetary medium characterised by a mean free path < 1 AU.

Fisk and Axford (1969) demonstrated that if $\kappa(r)$ increased with r, the anisotropy would decay more slowly; Burlaga (1971) developed a one-dimensional model (pitch-angles either 0 or 180°) in which $\kappa(r)$ essentially increased to infinity before the orbit of earth. Jokipii (1968) proposed that the decay

of anisotropy can be longer if the power spectrum of the interplanetary magnetic field falls off with frequency faster than f^{-1}, as this causes the particles to scatter more slowly through $90°$ pitch-angle.

As shown below, the anisotropy amplitude recorded by the 7.6 – 55 MeV energy channel of the UTD experiment on Explorer 41 for the event of 20 April, 1971 remained large and field aligned well into the decay portion of the intensity profile. A Monte Carlo technique was employed to calculate numerically the pitch-angle distributions, anisotropy amplitude and intensity of this solar cosmic ray event. With this flexible technique we were able to reproduce the anisotropy amplitude and intensity profiles in the given event, and infer certain propagation parameters which were consistent with the observations.

4.1   The Observational Data

In Figure 10, we show the hourly average values of the 7.6 – 55 MeV proton counting rate and anisotropy amplitude, δ, for the solar proton event of 20 April 1971. It can be seen that δ is $\gtrsim$ 100% for about 10 hours, that is, well into the decay of the event. Thus this event may be regarded as a counter-part of the "scatter-free" electron events described by Lin (1970). The maximum counting rate was mostly recorded by the octant centered on a direction $45°$W of the Earth-Sun line, in agreement with the nominal spiral field direction. The angular distribution in the plane of the ecliptic for a 10.9 minute data sample, 0152-0203 UT, 21 April is shown in Figure 11 and clearly illustrates the extreme collimation of the incoming particle flux, and the small amount of back scattering present at this time.

For this period, the satellite line of apsides was approximately 75° east of the Earth-Sun line. The satellite location in solar ecliptic coordinates is indicated at intervals of about 4 hours in Figure 10. At the onset of the event, the satellite is in close proximity to the average position of the bow shock for the 1963-1968 epoch as reported by Fairfield (1971). Clearly from Figure 10, a large anisotropy amplitude is detected well inside the average bow shock position and in fact, the anisotropy amplitude is destroyed only when the satellite approaches the average position of the magnetopause. Similar effects have been noted previously eg the 28 May 1967 and 16 December 1967 events reported by Bartley et al (1967). The available evidence (both published and unpublished) indicates that when the Explorer 34 and 41 satellites are located on the sunward side (i.e. X_{SE} is positive), it is possible to follow a field aligned anisotropy phase across the bow shock and close to the magnetopause without the character of the anisotropy being destroyed. (See Section 5 below). For the present analysis, the important point to note is that there is no evidence to indicate that the field aligned anisotropy is consistently prolonged by the proximity of the satellite to the bow shock or the magnetopause. To the contrary, the anisotropy amplitude is considerably reduced when the satellite approaches the magnetopause. We cannot state emphatically that the anisotropy amplitude inside the bow shock is exactly the same amplitude that would be measured by a satellite in interplanetary space. For the present analysis, we believe that the anisotropy amplitude presented in Figure 10 is valid i.e. close to the amplitude that would have been obtained in interplanetary space and if not exactly so, any correction would only result in enhancing the noted effect by increasing the anisotropy amplitude at late times in the event as the satellite

approaches the magnetopause.

The parent flare, of importance 1B and situated at S 06°, W 50°, began at 1924 UT with maximum phase at 1946 UT on 20 April 1971. It was accompanied by an X-ray burst in the 0 - 3°A range which began at 1920 UT and reached maximum at 1940 UT (Solar Geophysical Data, No. 326, Part II). In the 2-12 $^{\circ}$A range, the x-ray burst commenced at 1927 UT reaching a maximum phase at 1945 UT. It is difficult to give a precise onset time due to a 20 minute gap in the available particle data. The best estimate for particle arrival in the 7.6 - 55 MeV energy channel is 2135 UT giving a delay time of 109 minutes between the maximum phase of the flare and particle arrival time at earth orbit. Taking 11 MeV as a representative value of the particle energy in this channel, the calculated transit time for a 1.2 AU travel path is 65 minutes. As an extreme case, for 8 MeV particles the transit time is 77 minutes for the same distance. Hence, although the parent flare was very close to the foot of the nominal Archimedes spiral field line, the measured arrival time at earth orbit implies that if the particles were accelerated at or prior to the X-ray peak, then those first arriving at earth were delayed at least 32 minutes and probably 40 minutes in their escape from the acceleration region, or by their propagation along the field lines.

In the subsequent analysis of this event, it is assumed that any modification of the temporal profile due to corotation is negligible; that is, we assume a uniform particle population across an azimuth of $\sim$13° in the spiral field behind Earth after the onset of the event.

4.2   Results

A Monte Carlo technique was used to investigate the intensity and anisotropy amplitude at 1 AU for this particular solar proton event. This technique was introduced by Vernov et al. (1969) in a study of particle anisotropy, and subsequently developed by Palmer (1972, 1973) to explore the effects of sweeping of solar particles ahead of a shock wave, and to study the magnitude and rate of energy loss at 1 AU for different models of solar cosmic ray events.

Particles which are released one at a time from a point representing the sun are monitored as they propagate along radially diverging field lines. Pitch-angle scattering is incorporated by changing the pitch-angle (either isotropic or small-angle scatter) after the particle traverses a predetermined mean free path. Between scatterings the particle is assumed to follow guiding center motion. Time and pitch-angle are recorded when a particle crosses 1 AU. After a large number of particles has been processed the pitch-angle distribution, anisotropy, and omnidirectional intensity are extracted as a function of time.

Figure 10 shows the intensity and anisotropy profiles obtained from the Monte Carlo model superimposed on the observations. The best fit was obtained with a uniform $\kappa = 3.7 \times 10^{22} \mathrm{cm}^2 \mathrm{s}^{-1}$ in conjunction with an exponentially decaying source of e-folding time 7 hours, but only if the particle injection is assumed to have begun 1.5 hours after the X-ray peak.

The position of the free-escape boundary determines in part the rate of intensity decay; a value of 4 AU gives the best agreement shown in Figure 10.

5.0   Particle Anisotropy Measurements Close to the Earth's Magnetic Field

In two sections of this report, (viz 3.1 and 4.1), we have already referred to the particle anisotropy measurements and the proximity of the satellite location to the bow shock or the magnetopause. In this section, we will discuss this problem in more detail using data from the Explorer 34 for the event of 09 August, 1967. In particular, we will examine the field aligned phase of a particle event as the observing platform crosses the bow shock and approaches the magnetopause.

5.1   09 August, 1967 Event

The intensity-time profile, using hourly averages of the data for the low-energy proton event of 09 August, 1967 is shown in Figure 12. In Figure 13, we show, using 9.28 second averages of the data taken every 81.92 seconds, the rising portion of the event on the inbound pass of orbit 18 of Explorer 34. The relative counting rate of the 0.7 - 7.6 MeV energy level, together with the relative particle anisotropy amplitude and phase for this level, and the concurrent magnetic field data (field magnitude; ecliptic latitude, θ_m and ecliptic longitude ϕ_m, of the magnetic field vector; the standard deviation of the field in the X-direction of the solar ecliptic coordinate system) are shown in this figure.

The first encounter with the bow shock occurs at 0238 UT, 10 August while the final shock crossing occurs at 0350 UT, 10 August. The magnetopause crossing occurs at 0532 UT. The interesting point in this diagram is the substantial anisotropy observed between 0449 UT and 0521 UT. Clearly this anisotropy is field aligned (as may be seen from a comparison of panels (d) and (f)) even though the satellite is well inside the bow shock at this time. (approximate location $X_{SE} = 9.75$ R_e; $Y_{SE} = 5.36$ R_E; $Z_{SE} = 5.37$ R_E). The

amplitude of the anisotropy is comparable to that measured by Innanen and

Van Allen (1973) using Explorer 35 data for the same event. The amplitude

of the anisotropy begins to decrease at 0521 UT and by 0528 UT the character

of the anisotropy has changed completely. In Figure 14, we show the counting

rate from the proportional counter in our experimental package. At this

time, the proportional counter is just beginning to record magnetospheric

electrons (>70keV).

The conclusion that we can draw from these data, and from other events

is that while we cannot state explicitly that the anisotropy amplitude

measured inside the bow shock and close to the magnetopause is exactly the

same as that anisotropy which would have been measured in interplanetary space

nevertheless the character of the measured anisotropy (i.e. the field aligned

nature of the measurements) is not changed until the satellite is close to the

magnetopause and that the measured anisotropy is approximately the same as

that measured independently on another satellite in the interplanetary medium.

In Figures 15, 16 we show the data corresponding to Figures 13, 14 above,

for the outbound pass of orbit 19. The bow shock crossing occurs at 2039 UT,

10 August. As early as 1809 UT, the particle anisotropy is large, field

aligned and approximately equal in amplitude to the value obtained by Innanen

and Van Allen (1973). At this time the satellite coordinates are as follows:

$X_{SE} = 9.89 \ R_E$; $Y_{SE} = 6.36 \ R_E$; $Z_{SE} = -7.17 \ R_E$; which is close to the average

position of the magnetopause and obviously deep inside the bow shock. A

comparison of Figures 15 and 16 indicates that the increase in proton anisotropy

is almost coincident with the decrease in the proportional counter response as

the satellite leaves the trapped particle regime.

Similar analysis has been performed for a number of other particle events. The general conclusion drawn is that for the orbits of Explorer 34 and 41, it is possible to follow the character of the anisotropy i.e. whether the anisotropy is field aligned or otherwise, well inside the bow shock position. When the satellite is located deep in the magnetotail, any particle anisotropy is completely destroyed.

6.0   Concluding Remarks

(i)   A paper based on the work summarized in #2.1 has been submitted to Solar Physics.

(ii)   The material discussed in 2.2 is still under investigation with additional examples being sought in the currently available data.

(iii) A preliminary report of the data discussed in #3 will be presented in a report submitted to COSPAR/STP, edited by D. Smart and M. Shea (ACRL). A more complete analysis of these events, including a detailed comparison with concurrent magnetic field data is under way and will be submitted to a scientific journal for publication.

(iv)   A paper based on the data and analysis presented in #4 is currently in preparation and will be submitted to Solar Physics in April.

(v)   The data discussed in #5 is being further evaluated before it will be presented to the scientific community. Additional examples of the effect on the field aligned phase as the satellite approaches the earth's magnetic field will be examined before submitting this material for publication.

Acknowledgement

REFERENCES

Allum, F. R., Palmeira, R. A. R., Rao, U. R., McCracken, K. G., Harries, J. R., and Palmer, I. D.: 1971, Solar Phys. 17, 241.

Allum, F. R., Palmeira, R. A. R., McCracken, K. G., Rao, U. R. Fairfield, D. H., and Gleeson, L. J.: 1973, Proc. 13th International Cosmic Ray Conference, page 1432.

Allum, F. R., Palmeira, R. A. R., McCracken, K. G., Rao, U. R., Fairfield, D. H., and Gleeson, L. J.: 1974 Submitted to Solar Physics.

Axford, W. I.: 1971, Proc. Symp. on Solar-Terrestrial Physics, Leningrad.

Bartley, W. C., McCracken, K. G., Rao, U. R., Harries, J. R., Palmeira, R. A. R., and Allum, F. R.: 1971, Solar Physics 17, 219.

Bryant, D. A., Cline, T. L., Desai, U. D., and McDonald, F. B.: 1962, J. Geophys. Res. 67, 4983.

Bryant, D. A., Cline, T. L. Desai, U. D., and McDonald, F. B.: 1965, Astrophys. J., 141, 478.

Fairfield, D. H.: 1971, J. Geophys. Res. 76, 6700.

Fisk, L. A. and Axford, W. I.: 1969, Solar Phys. 7, 486.

Innanen, W. G., and Van Allen, J. A.: 1973, J. Geophys. Res., 78, 1019.

Jokipii, J. R.: 1968, Astrophys. J., 152, 671.

Lin, R. P.: 1970, Solar Phys. 15, 453.

McCracken, K. G., Rao, U. R., Bukata, R. P., and Keath, E. P.: 1971, Solar Phys. 18, 100.

Palmer, I. D.: 1972, Solar Phys. 27, 466.

Palmer, I. D.: 1973, Solar Phys. 30, 235.

Rao, U. R., McCracken, K. G., and Bukata, R. P.: 1967, J. Geophys. Res. 72, 4325.

Rao, U. R., McCracken, K. G., Allum, F. R., Palmeira, R. A. R., Bartley, W. C., and Palmer, I. D.:   1971, Solar Phys. 19, 209.

Vernov, S. N., Chudakov, A. E., Vakulov, P. V., Gorchakov, E. V., Kontor, N. N., Logachev, Y. I., Lyubimov, G. P. Pereslegina, N. V., and Timofeev, G. A.:   1969, Geomagn. i Aeron. IX, 6, 775.

Figure Captions

Figure 1:   Temporal variation of the counting rate for the 0.7 - 55

MeV proton energy channel during the interval 27 May to

24 June 1972. Hourly averages of the data were used in

preparation of this figure.

Figure 2:   Illustrating the general relationship between the

particle anisotropy and the concurrent magnetic field for

the period 0300 UT; 06 June and 0300 UT, 08 June, 1972.

The vector triangles showing the convective and diffusive

components of the particle anisotropy together with the

resultant particle anisotropy are given in panels (c) and (d).

Figure 3:   Illustrating a possible configuration for the interplanetary

magnetic field to explain the observed particle and magnetic

field data shown in Figure 2.

Figure 4:   Temporal variation of the counting rate for the 7.6 - 55

MeV proton energy channel during the interval 08 June -

20 June 1972. Hourly averages of the data were used in the

preparation of this figure.

Figure 5:   The hourly anisotropy vector diagram for the event of 08

June 1972.

Figure 6:   The angular distribution of 0.7 - 7.6 MeV protons in the

plane of the ecliptic averaged over 10.9 minute time

intervals; (a) During the field aligned phase of the 08

June event; (b) During the field aligned phase of the 16

June event; (c) Immediately preceeding the arrival of the

shock front on 17 June; (d) Immediately after the
arrival of the shock front on 17 June; (e) and (f)
During the period when a bidirectional distribution is
detected.

Figure 7:   The hourly anisotropy vector diagram for the event of
                16 June, 1972.

Figure 8:   Temporal variations of protons in the energy ranges
                (a) 0.7 - 7.6 MeV, (b) 7.6 - 55 MeV and (c) >35 MeV
                following the passage of the interplanetary shock front
                which produced the sudden commencement at 1312 UT, 17 June
                1972. The Forbush decrease observed at the higher energies
                and the energetic storm particle event observed at the
                lower energies are clearly evident. The period when bi-
                directional anisotropies are observed is also indicated.

Figure 9:   Temporal variation of the anisotropy amplitude and phase
                of the 0.7 - 7.6 MeV protons at the time of the passage
                of the interplanetary shock front across the satellite
                location on 17 June 1972. These data were obtained during
                9.28 second accumulation periods every 81.92 seconds.

Figure 10:   The relative counting rate of the 7.6 - 55 MeV proton
                channel (a) and the corresponding anisotropy amplitude (b)
                for the 20 April, 1971 event. Hourly averages of the data

were used in the preparation of this diagram. The

crosses indicate the Monte Carlo fit to the experimental

data.

Figure 11: Illustrating the octant distribution for a 10.9 minute

data sample, 0152 - 0203 UT, 21 April, 1971, for the

0.7 - 7.6 MeV and 7.6 - 55 MeV energy channels. The

direction of the center of each octant relative to the

earth-sun line is indicated at the top of the diagram.

Figure 12: The intensity-time profile for the 0.7 - 7.6 MeV energy

channel for the event of 09 August, 1967. Hourly averages

of the data were used in the preparation of this diagram.

Figure 13: Fine time scale particle and magnetic field data for the

inbound pass of orbit 18, Explorer 34, during the field

aligned phase of the low energy proton event of 09 August,

1967.

(a) The relative count rate of the 0.7-7.6 MeV channel;

data samples averaged over 9.28 seconds taken every 81.92

seconds.

(b) The magnitude of the magnetic field vector. Only the

data points which correspond to the times at which the

particle data are taken are shown in this and the other

panels ((e), (d), (e)) of this diagram.

(c) The solar ecliptic latitude, ϕ_m, of the magnetic field

vector.

(d) The solar ecliptic longitude ϕ_m of the magnetic

field vector. ϕ_m gives the direction in the plane of the

ecliptic in which the magnetic field is pointing and is

measured positive East (E) of the earth-sun line.

(e) Variance of the magnetic field in the X-axis of

the solar ecliptic coordinate system.

(f) The azimuth, ϕ_{cr} of the 0.7 - 7.6 MeV proton flux

during this time period. ϕ_{cr} is the direction in the

ecliptic plane from which the maximum particle flux is

observed and is measured positive West (W) of the earth-

sun line.

(g) The anisotropy amplitude, expressed as a percentage,

for the 0.7 - 7.6 MeV proton flux during this period.

Figure 14:   The relative count rate of the proportional counter on

the inbound pass, orbit 18, of Explorer 34. The electron

energy threshold for this counter is 70 keV.

Figure 15:   Fine-time-scale particle and magnetic field data for the

outbound pass of orbit 19, Explorer 34 during the field

aligned phase of the low energy proton event of 09 August,

1967.

(a) The magnitude of the magnetic field vector. Only

the data points which correspond to the times at which

the particle data are taken, are shown in this and the

other panels ((b), (c), (d)) of this diagram.

(b) The solar ecliptic latitude, θ_m, of the magnetic field vector.

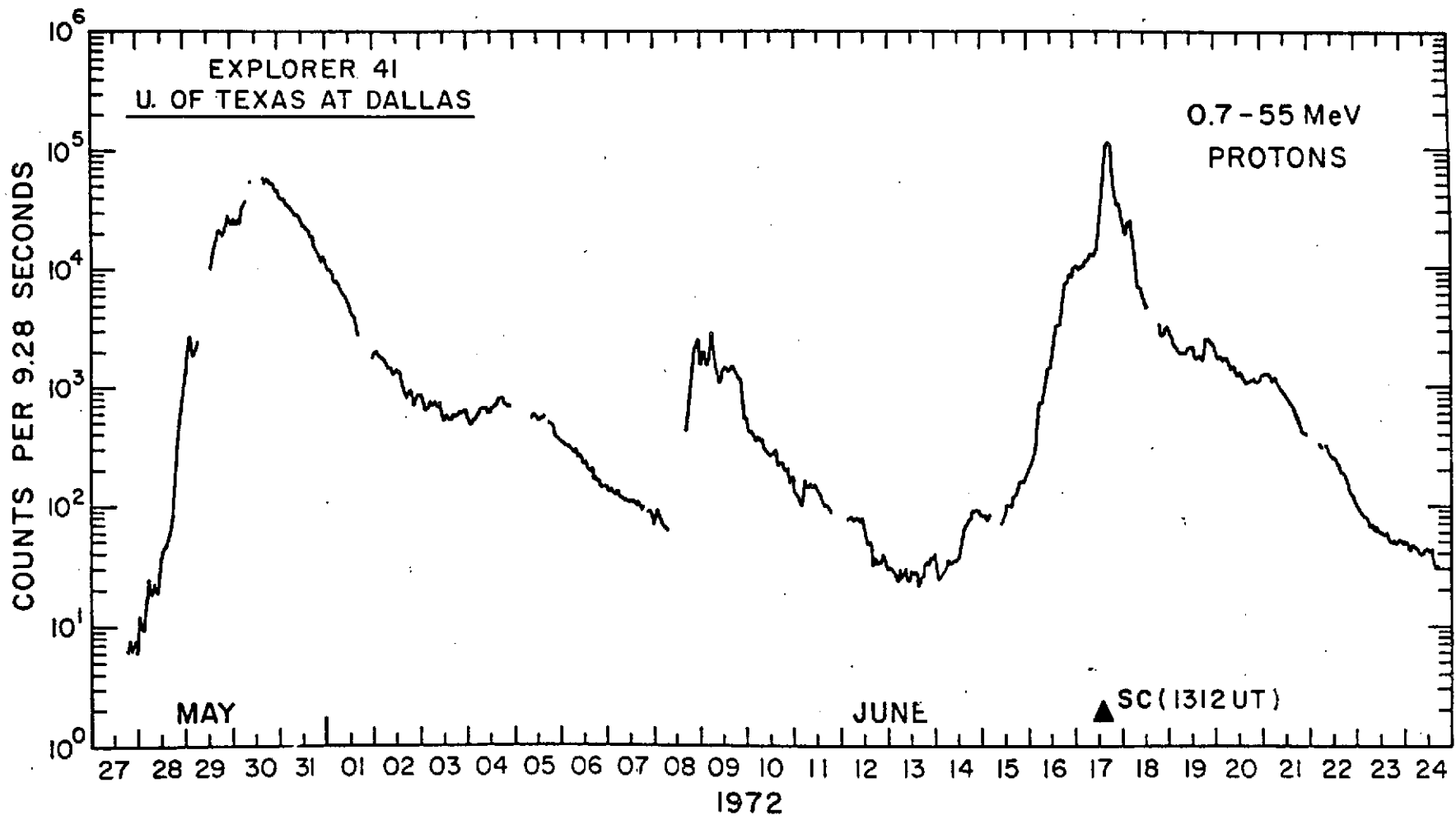(c) The solar ecliptic longitude, ϕ_m, of the magnetic field vector.

(d) Variance of the magnetic field in the X-axis of the solar ecliptic coordinate system.

(e) The azimuth, ϕ_{cr}, of the 0.7 - 7.6 MeV proton flux during this time period. The data points are taken over 9.28 second intervals every 81.92 seconds.

(f) The anisotropy amplitude, expressed as a percentage, for the 0.7 - 7.6 MeV proton flux during this period.

Figure 16:   The relative count rate of the proportional counter on the outbound pass, orbit 19, of Explorer 34.
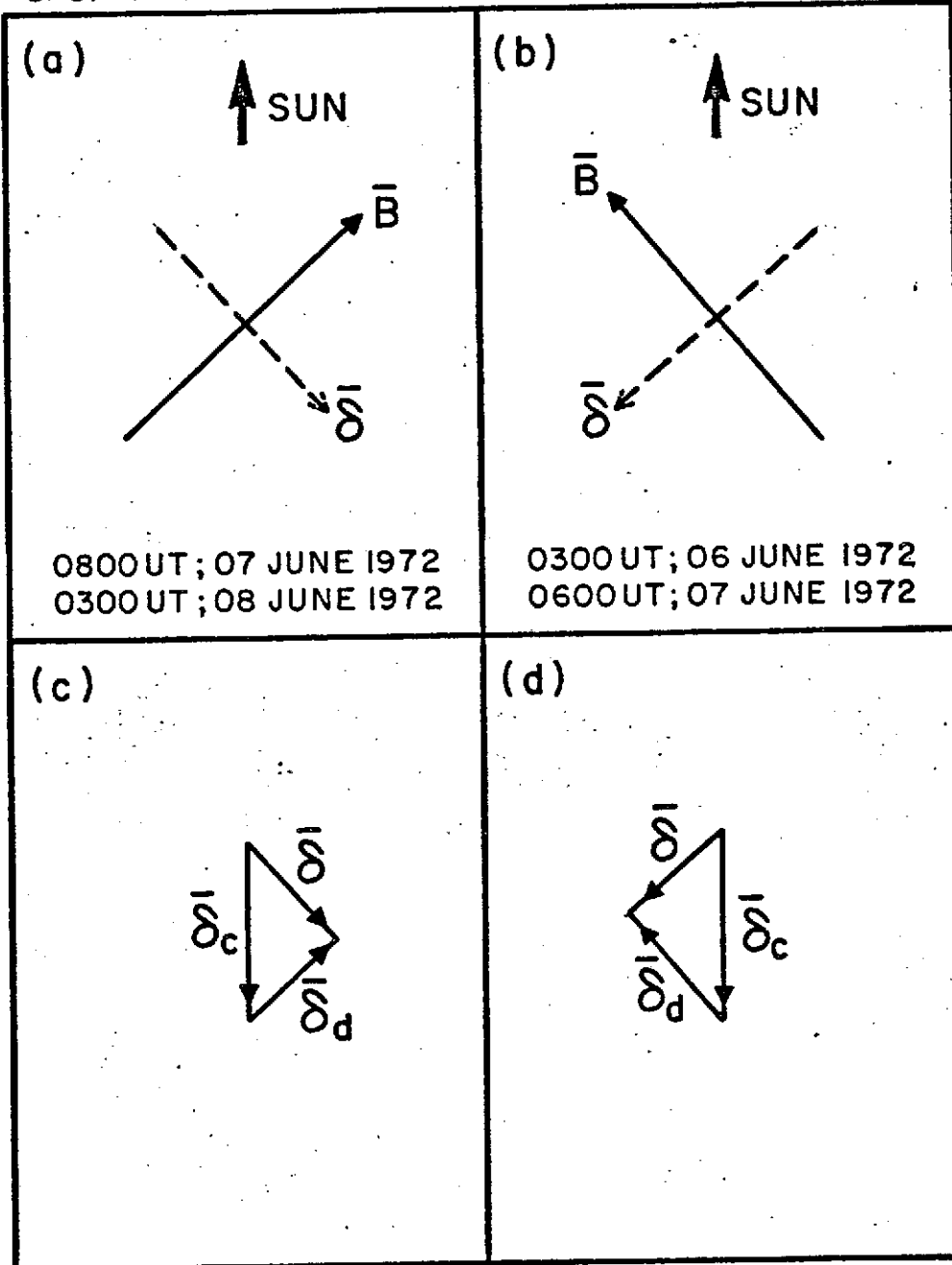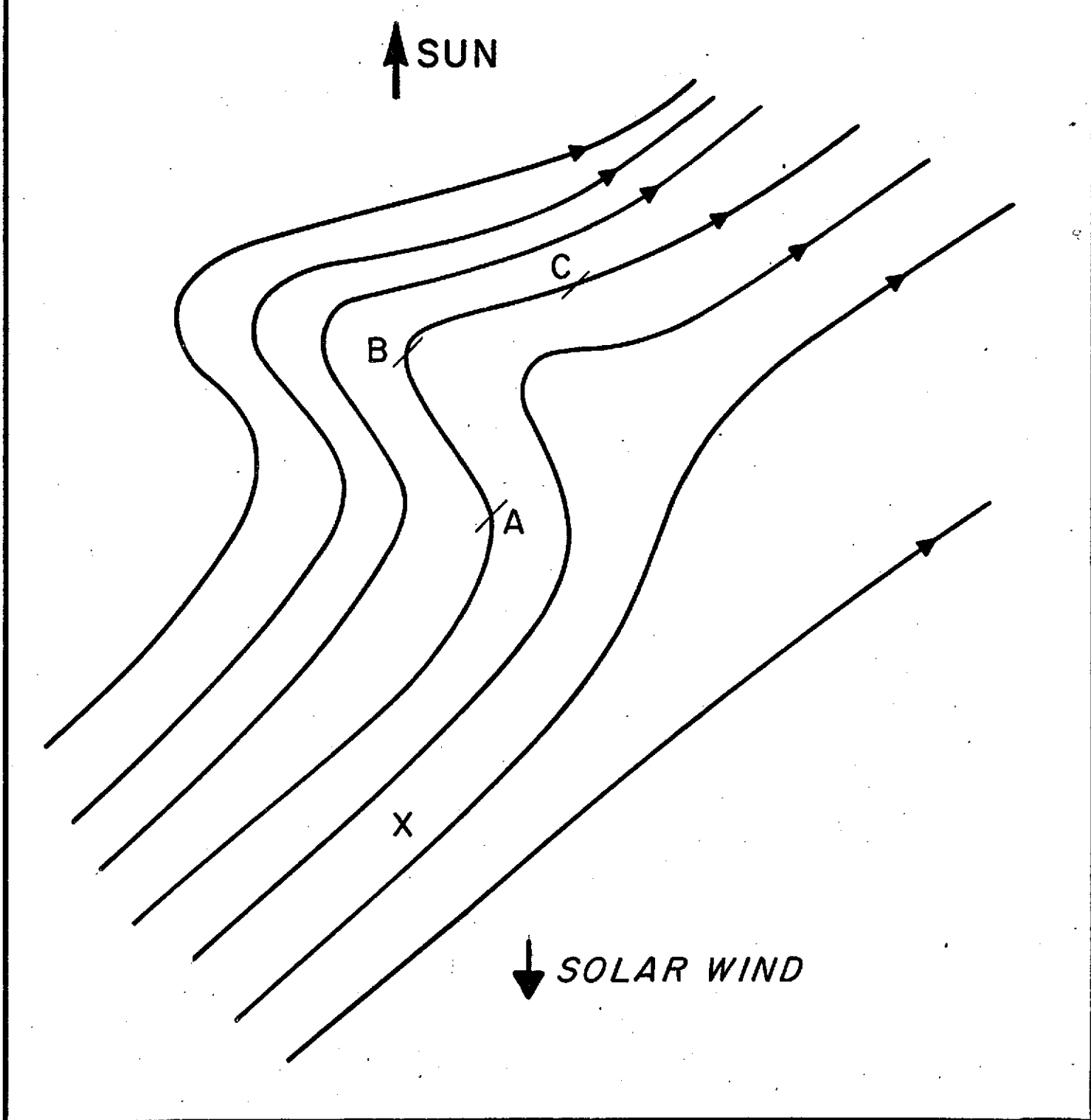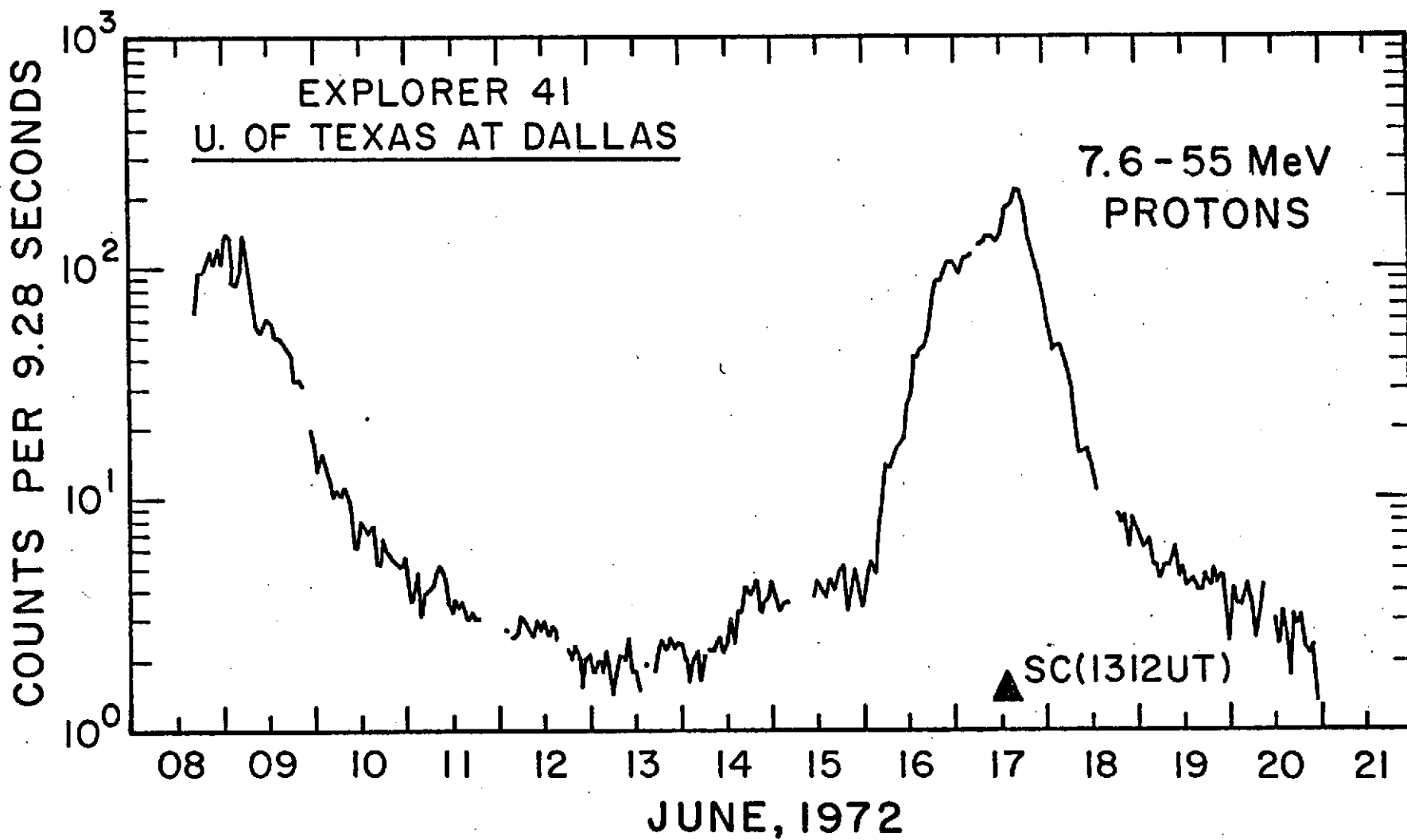
FIGURE 1

EXPLORER 41
U. OF TEXAS AT DALLAS

0.7 – 55 MeV
PROTONS

COUNTS PER 9.28 SECONDS

MAY

JUNE

SC (1312 UT)

27 28 29 30 31 01 02 03 04 05 06 07 08 09 10 11 12 13 14 15 16 17 18 19 20 21 22 23 24

1972

-29-

FIGURE 2

U. OF TEXAS AT DALLAS

SUN

C

B

A

X

SOLAR WIND

FIGURE 3

EXPLORER 41
U. OF TEXAS AT DALLAS

7.6 - 55 MeV
PROTONS

SC(1312UT)

COUNTS PER 9.28 SECONDS

JUNE, 1972

FIGURE 4

EXPLORER 41
U. OF TEXAS AT DALLAS

ANISOTROPY VECTOR
DIAGRAM

0.7 – 7.6 MeV
PROTONS

1800 UT
08 JUNE

0000 UT
09 JUNE

TO SUN

0600 UT
09 JUNE

1200 UT
09 JUNE

1800 UT
09 JUNE

DATA GAP

0600 UT
10 JUNE

1200 UT
10 JUNE

0600 UT
11 JUNE

1400 UT
11 JUNE

0000 UT
11 JUNE

1800 UT
10 JUNE

0400 UT
12 JUNE

DATA GAP
ORBIT PERIGEE

08 – 12 JUNE, 1972

1200 UT
12 JUNE

100%

ANISOTROPY SCALE

FIGURE 5

–33–

FIGURE 6

EXPLORER 41
U. OF TEXAS AT DALLAS

1100 UT
15 JUNE

0300 UT
16 JUNE

0600 UT
16 JUNE

1200 UT
16 JUNE

1800 UT
16 JUNE

TO SUN

0500 UT
17 JUNE

0000 UT
17 JUNE

SUDDEN
COMMENCEMENT
1312 UT, 17 JUNE

1200 UT
17 JUNE

0.7 – 7.6 MeV
PROTONS

1600 UT
17 JUNE

DATA GAP

2000 UT
17 JUNE

0700 UT
18 JUNE

0000 UT
19 JUNE

DATA GAP
ORBIT PERIGEE

0600 UT
19 JUNE

15 – 24 JUNE, 1972

1200 UT
19 JUNE

0000 UT
20 JUNE

1800 UT
19 JUNE

1200 UT
20 JUNE

0600 UT
20 JUNE

ANISOTROPY VECTOR
DIAGRAM

1600 UT
21 JUNE

0200 UT
21 JUNE

DATA GAP
ORBIT PERIGEE

1200 UT
22 JUNE

0000 UT
23 JUNE

1200 UT
23 JUNE

1800 UT
23 JUNE

1600 UT
24 JUNE

100%

ANISOTROPY SCALE

FIGURE 7

FIGURE 8

FIGURE 9

EXPLORER 41
U. OF TEXAS AT DALLAS

ANISOTROPY DATA
0.7 - 7.6 MeV
PROTONS

ANISOTROPY AMPLITUDE (%)

PHASE (DEG.)

100

50

0

0°

WEST

180°

EAST

0°

SC 1312 UT

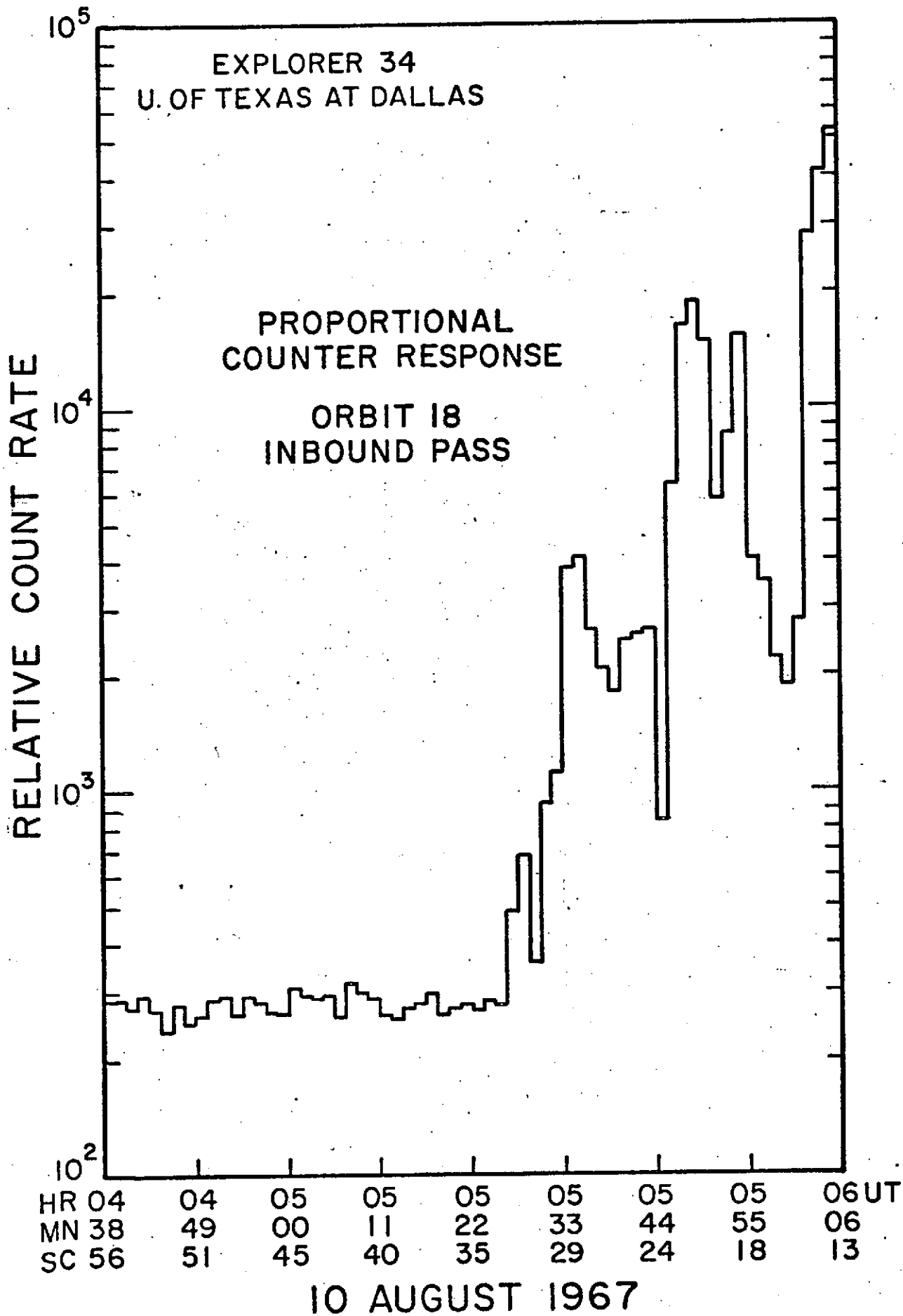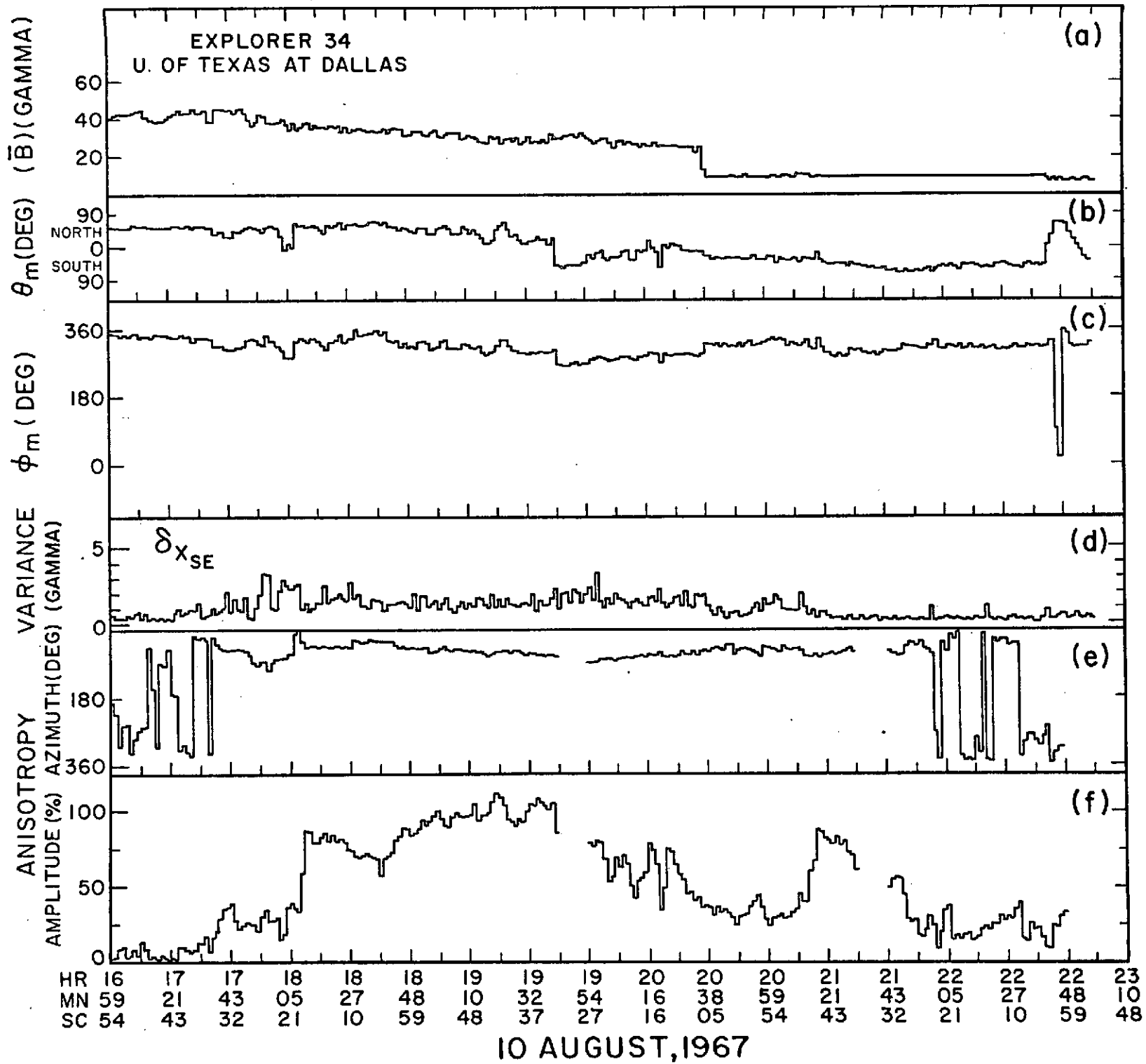| Hr	11	11	12	11	12	12	12	13	13	13	13	13	13	14
Mn	46	57	08	19	30	41	52	03	14	24	35	46	57	08
Sc	46	40	35	29	24	18	13	07	02	57	51	46	40	35

17 JUNE 1972
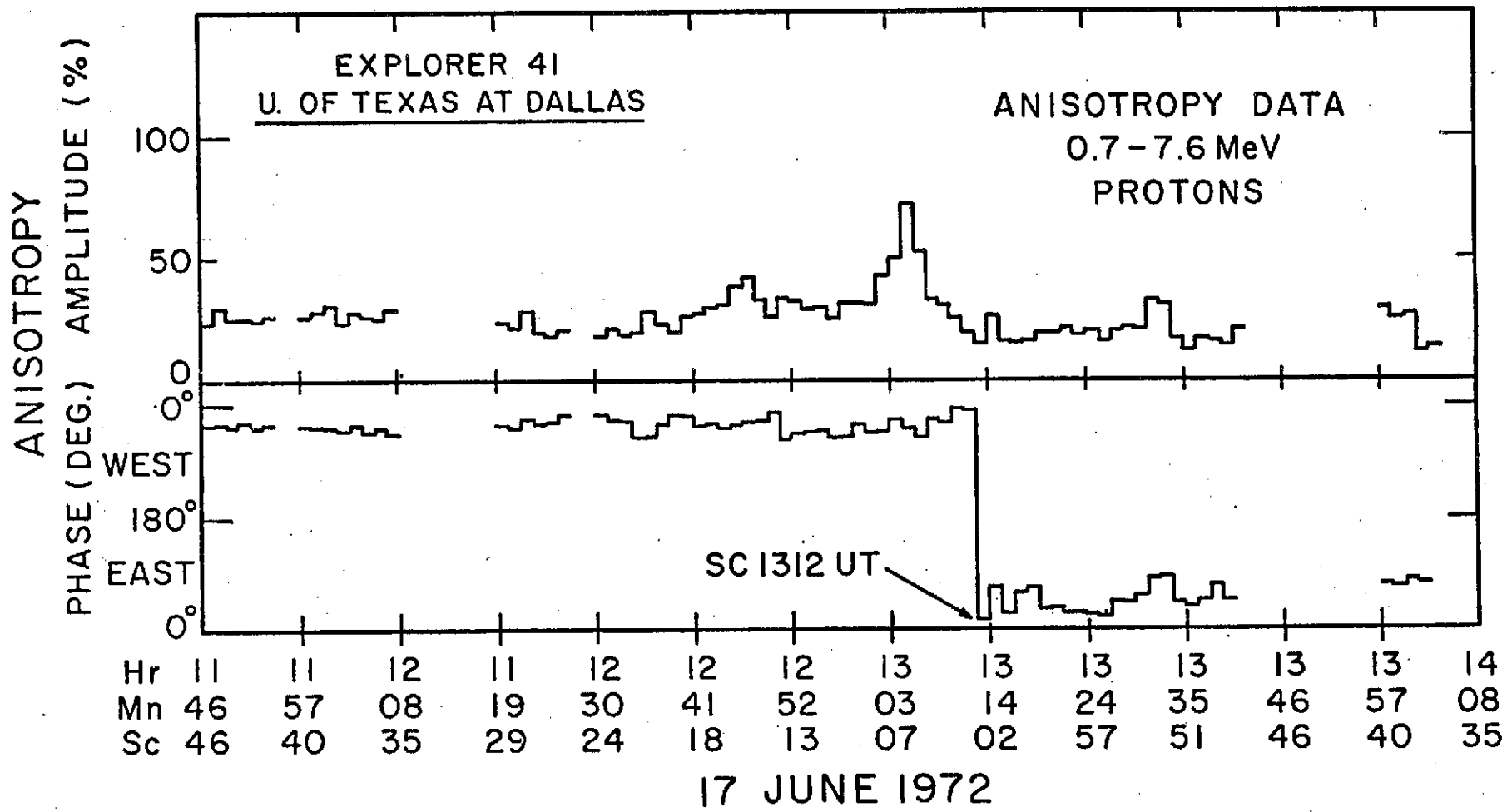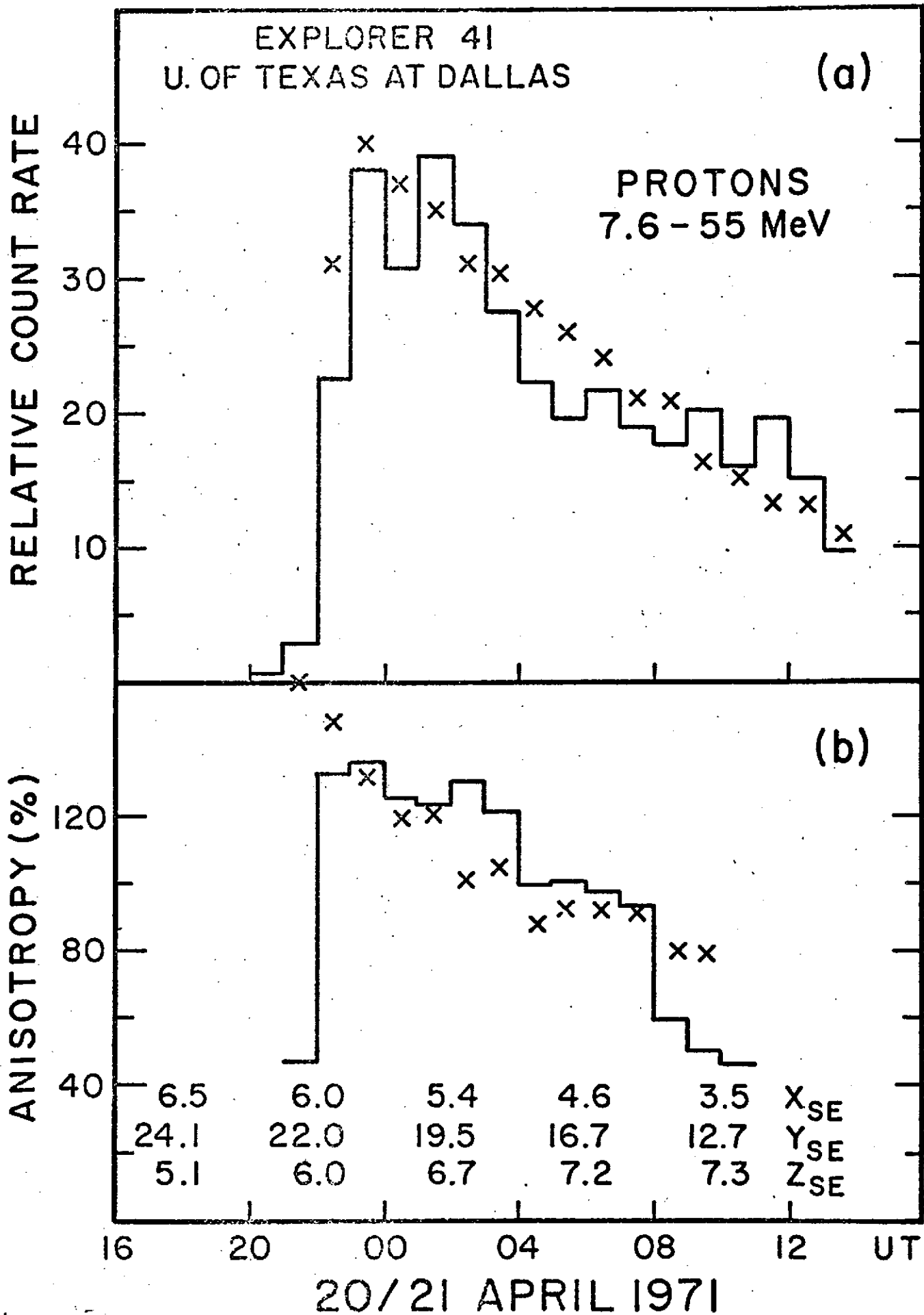
FIGURE 10

FIGURE 11

FIGURE 12

EXPLORER 34
U. OF TEXAS AT DALLAS

DATA GAP

0.7-7.6 MeV PROTONS

2B, (S24, E32)

DATA GAP

UT

PROTONS CM⁻² SEC⁻¹ SR⁻¹

AUGUST, 1967

-40-

FIGURE 13

-42-

EXPLORER 34
U. OF TEXAS AT DALLAS

0.7 – 7.6 MeV
PROTONS

AUGUST, 1967

FIGURE 14

FIGURE 15

EXPLORER 34
U. OF TEXAS AT DALLAS

10 AUGUST, 1967

FIGURE 16